

FORM 443

BALLISTIC RESEARCH LABS ABERDEEN PROVING GROUND MD F/G 29/4
COMPUTATIONAL PARAMETRIC STUDY OF THE AERODYNAMICS OF SPINNING --ETC(U)
JUN 80 W B STUREK, D C MYLIN, C C BUSH

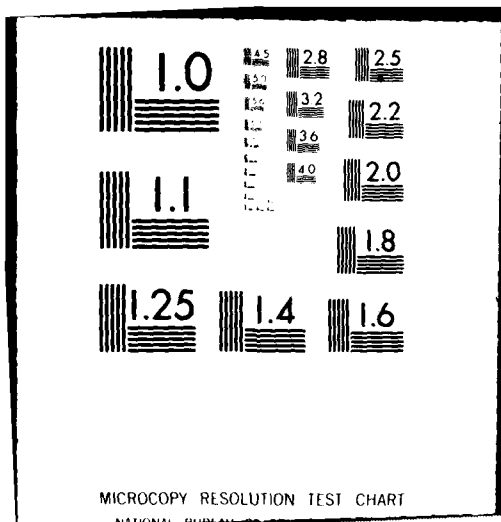
UNCLASSIFIED

NL

10-1
40
478-1054



END
DATE
FILMED
11-80
DTIC



MICROCOPY RESOLUTION TEST CHART

NATIONAL BUREAU OF STANDARDS-1963-A

AD A090443

12/15

LEVEL #

DTIC ELECTE
OCT 20 1980

A

6 COMPUTATIONAL PARAMETRIC STUDY OF THE AERODYNAMICS OF SPINNING SLENDER BODIES AT SUPERSONIC SPEEDS

10 WALTER B. STUREK DONALD C. MYLIN Mr.,
CLARENCE C. BUSH Mr.
U.S. Army Ballistic Research Laboratory
Aberdeen Proving Ground, Maryland 21005

11

I. INTRODUCTION

Recent trends in projectile design have led to shapes with greater length and more slender ogives. Unexpected flight stability problems have been encountered due to decreased aerodynamic stability of these new shapes. Clearly, conventional aerodynamic predictive capabilities were not adequate. In an effort to avoid these problems in the future, the Ballistic Research Laboratory has been developing advanced numerical computational techniques for computing projectile aerodynamic characteristics to improve shell design technology.

Substantial progress has been made in the past 10 years in the development of aerodynamic computational techniques and in the availability of high speed digital computers. This progress has made it possible to begin to use advanced finite-difference computational techniques to perform parametric aerodynamic studies for evaluation of proposed design concepts.

The use of advanced numerical computational techniques for a parametric study is difficult to justify to compute only static aerodynamic parameters since cheaper, less complex techniques such as Ref. (1), (2) and (3) are available. However, if dynamic derivatives such as Magnus and pitch damping are considered important and if viscous drag is of interest, then the advanced computation techniques are justified and, in fact, must be used. This paper reports the initial results of an ongoing research effort at BRL to form an advanced aerodynamic computation capability that will provide the shell designer with a complete package of static and dynamic aerodynamic coefficients for use in design studies.

This document has been approved for public release; its distribution is unlimited.

DDC FILE COPY

309

050750

JM

80 10 17 021

II. COMPUTATIONAL TECHNIQUES

Scope of Effort

Three dimensional finite-difference flow field computational techniques for inviscid and turbulent viscous flow have been applied to generate a comprehensive set of aerodynamic coefficients for cone-cylinder (CC), tangent-ogive-cylinder (TOC), and secant-ogive-cylinder (SOC) body configurations. The model geometries considered in this study are shown in Figure 1. Body lengths up to seven calibers

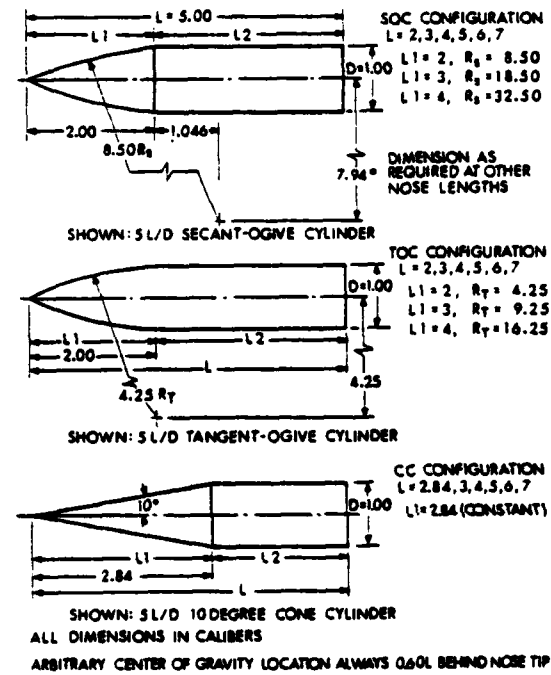


Figure 1. Model Geometries

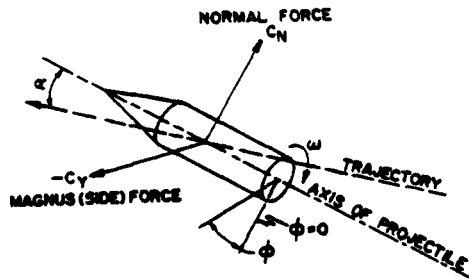
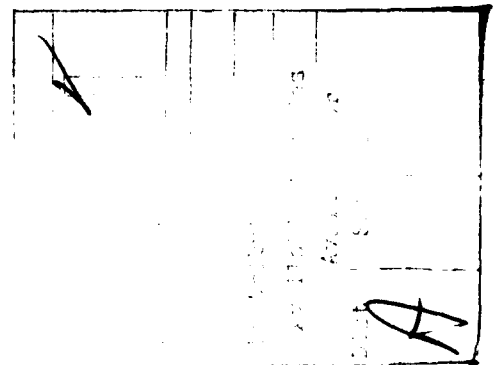


Figure 2. Magnus and Normal Forces on Spinning Projectile

and ogive lengths of two, three, and four calibers have been considered. The aerodynamic coefficients computed are pitching moment, normal force, center of pressure, Magnus moment, Magnus force, Magnus center of pressure, form and viscous drag, roll damping and pitch damping. The sign convention for the pitch plane and Magnus forces is shown in Figure 2. All aerodynamic coefficients are computed in a conceptually exact manner. The only empirical input is that required for the modeling of turbulent eddy viscosity.

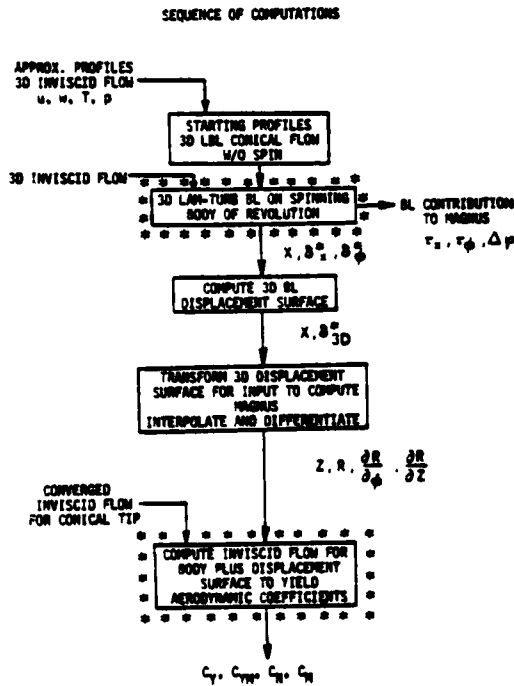
The computations have been carried out for a Mach number range of $1.75 \leq M \leq 5$. These computations were all performed for an angle of attack of 1° , a nondimensional spin rate (PD/V) of 0.19, and for sea level atmospheric free-stream conditions. Specific comparisons to wind tunnel data were made for the tunnel operating conditions.



310

Coupled Inviscid-Viscous Computations

The sequence of computations which are run in order to compute the static aerodynamic parameters, including turbulent viscous effects, is shown in Figure 3. Each block represents a separate computer code. These codes have been combined using the overlay technique on the BRL Cyber computer. The two main codes are those which compute three dimensional turbulent boundary layer development and three dimensional inviscid flow.



The computation of the effects of viscosity is of crucial importance when such parameters as roll damping, Magnus, and drag are of interest. The technique employed here is a fully implicit, finite difference numerical scheme developed by Dwyer⁽⁴⁾. This technique takes into consideration the changes in direction of the cross-flow velocity that occur on the side of the shell where the inviscid cross-flow opposes the surface spin.

The equations solved are the basic equations defining the three-dimensional compressible, turbulent boundary-layer flow over a body of revolution described by the relation $r = r(x)$. The coordinate system is shown in Figure 4.

Figure 3. Sequence of Computations

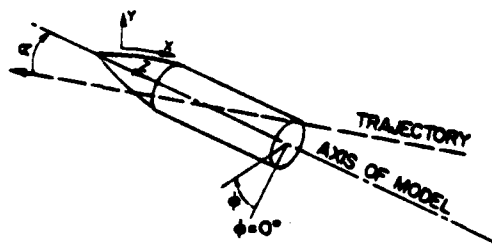


Figure 4. Coordinate System

311

Continuity

$$\frac{\partial}{\partial x} (r\bar{\rho}\bar{u}) + \frac{\partial}{\partial y} (r\bar{\rho}\bar{v}) + \frac{\partial}{\partial \phi} (r\bar{\rho}\bar{w}) = 0 \quad (1)$$

x momentum

$$\bar{\rho} \left[\bar{u} \frac{\partial \bar{u}}{\partial x} + \hat{v} \frac{\partial \bar{u}}{\partial y} + \frac{\bar{w}}{r} \frac{\partial \bar{u}}{\partial \phi} - \frac{\bar{w}^2}{r} \frac{\partial r}{\partial x} \right] = - \frac{\partial \bar{p}_e}{\partial x} + \frac{\partial}{\partial y} \left[\mu \frac{\partial \bar{u}}{\partial y} - \overline{\rho u'v'} \right] \quad (2)$$

 ϕ momentum

$$\bar{\rho} \left[\bar{u} \frac{\partial \bar{w}}{\partial x} + \hat{v} \frac{\partial \bar{w}}{\partial y} + \frac{\bar{w}}{r} \frac{\partial \bar{w}}{\partial \phi} + \frac{\bar{u}\bar{w}}{r} \frac{\partial r}{\partial x} \right] = - \frac{1}{r} \frac{\partial \bar{p}_e}{\partial \phi} + \frac{\partial}{\partial y} \left[\mu \frac{\partial \bar{w}}{\partial y} - \overline{\rho v'w'} \right] \quad (3)$$

Energy

$$\begin{aligned} \bar{\rho} \left[\bar{u} \frac{\partial \bar{h}}{\partial x} + \hat{v} \frac{\partial \bar{h}}{\partial y} + \frac{\bar{w}}{r} \frac{\partial \bar{h}}{\partial \phi} \right] &= \bar{u} \frac{\partial \bar{p}_e}{\partial x} + \frac{\bar{w}}{r} \frac{\partial \bar{p}_e}{\partial \phi} + \mu \left[\left(\frac{\partial \bar{u}}{\partial y} \right)^2 + \left(\frac{\partial \bar{w}}{\partial y} \right)^2 \right] \\ &- \overline{\rho u'v'} \frac{\partial \bar{u}}{\partial y} - \overline{\rho v'w'} \frac{\partial \bar{w}}{\partial y} + \frac{\partial}{\partial y} \left[\frac{\mu}{Pr} \frac{\partial \bar{h}}{\partial y} - \overline{\rho v'h'} \right] \end{aligned} \quad (4)$$

where $\hat{v} = \bar{v} + \overline{\rho'v'}/\bar{\rho}$ and the bar indicates a time-averaged quantity.

In order to obtain closure of this system of equations, the following models of the turbulence terms have been introduced:

Turbulent shear stress

$$- \overline{\rho u'v'} = - \overline{\rho v'w'} = \bar{\rho} \ell^2 \left[\left(\frac{\partial \bar{u}}{\partial y} \right)^2 + \left(\frac{\partial \bar{w}}{\partial y} \right)^2 \right] = \epsilon \left[\left(\frac{\partial \bar{u}}{\partial y} \right)^2 + \left(\frac{\partial \bar{w}}{\partial y} \right)^2 \right]^{1/2}$$

where ϵ is introduced as the turbulent viscosity and the mixing length, $\ell = 0.09 \delta \tanh[(0.4/0.09)(y/\delta)]$. Van Driest damping is used to account for the effect of the laminar sublayer.

Turbulent heat transfer

$$- \overline{\rho v'h'} = \frac{k_t}{c_p} \frac{\partial \bar{h}}{\partial y}$$

The turbulent Prandtl number is introduced as

$$Pr_t = c_p \epsilon / k_t = 0.90$$

The three-dimensional displacement surface is not merely the vector sum of the longitudinal and circumferential components of the boundary-layer displacement thickness. Instead, the differential equation derived by Moore⁽⁵⁾:

$$\frac{\partial}{\partial x} [\rho_e u_e r (\delta_{3-D}^* - \delta_x^*)] + \frac{\partial}{\partial \phi} [\rho_e w_e (\delta_{3-D}^* - \delta_\phi^*)] = 0 \quad (5)$$

must be solved for δ_{3-D}^* , the three-dimensional boundary-layer displacement thickness where

$$\delta_x^* = \int_0^\delta \left(1 - \frac{\rho u}{\rho_e u_e} \right) dy \quad \delta_\phi^* = \int_0^\delta \left(1 - \frac{\rho w}{\rho_e w_e} \right) dy$$

With a body fixed coordinate system, the gas dynamic equations for inviscid flow can be written as

$$E_z + F_r + G_\phi + H = 0 \quad (6)$$

where the flux vectors E, F, G, and H are

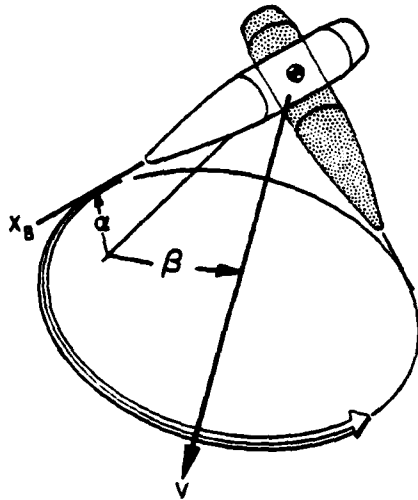
$$E = \begin{bmatrix} \rho u \\ \rho u^2 + p \\ \rho uv \\ \rho uw \end{bmatrix} \quad F = \begin{bmatrix} \rho v \\ \rho uv \\ \rho v^2 + p \\ \rho vw \end{bmatrix} \quad G = \frac{1}{r} \begin{bmatrix} \rho w \\ \rho uw \\ \rho vw \\ \rho w^2 + p \end{bmatrix} \quad H = \begin{bmatrix} \rho v \\ \rho uv \\ \rho (v^2 - w^2) \\ 2\rho vw \end{bmatrix}$$

These equations are solved using MacCormack's⁽⁶⁾ two-step, predictor-corrector finite difference scheme. The unique feature of the program used here, which was developed by Sanders⁽⁷⁾ for the Magnus problem, is that the flow field is computed about an axisymmetric model plus displacement surface. Due to the distortion of the viscous layer caused by interaction of the surface spin, the effective aerodynamic shape has no plane of symmetry.

The flow field variables resulting from these computation steps have been developed to yield the following aerodynamic coefficients--pitching moment, normal force, center of pressure, Magnus force, Magnus moment, Magnus center of pressure, form drag, viscous drag, and roll damping. The computational time for a single body configuration and flow field condition is approximately ten minutes on a CDC 7600 computer.

Coning Motion Computations

In order to compute the effective pitch damping, the technique developed by Schiff⁽⁸⁾ is used. This computational technique relates the side force on a body undergoing a coning motion about the CG location to the pitch damping ($C_{M_q} + C_{M_\alpha}$), see Figure 5.



The numerical technique is MacCormack's⁽⁶⁾ predictor-corrector, explicit marching scheme. This computation involves the solution of the Euler equations including terms for Coriolis ($2\rho \times \bar{\Omega} \times \bar{v}$) and centrifugal [$\rho \bar{\Omega} \times (\bar{\Omega} \times \bar{r})$] forces in a body fixed coordinate system. For this case, the H vector in equation 6 becomes

Figure 5. Coning Motion About Center of Gravity

$$H = \frac{1}{r} \begin{bmatrix} \rho v \\ \rho uv + \rho r [2(\omega_2 w - \omega_3 v) + \omega_1 \omega_2 r - x(\omega_2^2 + \omega_3^2)] \\ \rho(v^2 - w^2) + \rho r [2(\omega_3 u - \omega_1 w) + \omega_1 \omega_2 x - r(\omega_1^2 + \omega_3^2)] \\ 2\rho vw + \rho r [2(\omega_1 v - \omega_2 u) + \omega_3(\omega_2 r + \omega_1 s)] \end{bmatrix}$$

where ω_1 , ω_2 , and ω_3 are the components of the angular velocity vector $\dot{\theta}$ resolved in the z, r, and ϕ directions, respectively.

For the case of a steady coning motion, the flow field is time-invariant in the body-fixed coordinate system. The effective pitch damping ($C_{M_q} + C_{M_\alpha}$) is determined using the relation

$$C_{Y_{\dot{\theta}}} \approx \sin\sigma (C_{M_q} + C_{M_{\dot{\alpha}}}) \quad (7)$$

where $C_{Y_{\dot{\theta}}}$ = side force at coning rate $\dot{\theta}$ and effective angle of attack σ , which is valid for small values of σ and $\dot{\theta}$. Thus a dynamic aerodynamic parameter is determined using a steady flow field computation. This is a potentially very useful tool for the exterior ballisticians. The computation time is approximately 90 seconds on a CDC 7600 computer for the body configurations in this study.

III. RESULTS

Comparisons to Experiment

Detailed comparisons of the computations to experimental data for turbulent boundary layer profile characteristics, wall pressure measurements and Magnus force are reported in Ref. (9). Comparisons shown here will be limited to the aerodynamic coefficients of interest.

Examples of comparisons of the computed results to experimental data are presented in Figures 6 through 10. The comparisons for pitch plane static parameters shown in Figures 6, 7 and 8 indicate excellent agreement. The limited comparison for Magnus in Figure 9 indicates acceptable agreement if allowance is made for the small magnitude of the Magnus effect and the variance between the wind tunnel and range experimental measurements. A comparison between computation and experiment for pitch damping is shown in Figure 10. The experimental point, which is for an L/D of 5.12 and cone angle of 9.52° , shows excellent agreement with the trend of the computed results. In general, it is felt that the numerical computations do provide an accuracy for the aerodynamic coefficients that is within the uncertainty of our ability to determine these coefficients experimentally. However, it is felt that a broader scope of comparison for the aerodynamic coefficients between experiment and computation is of interest and increased effort to accomplish this is underway.

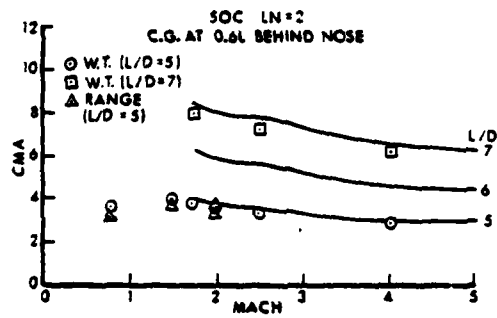


Figure 6. Pitching Moment, Comparison with Experiment

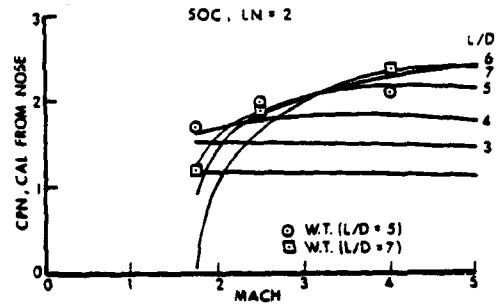


Figure 7. Center of Pressure, Comparison with Experiment

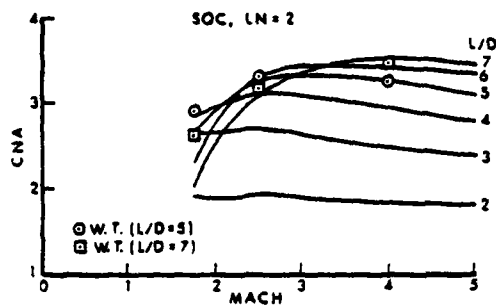


Figure 8. Normal Force, Comparison with Experiment

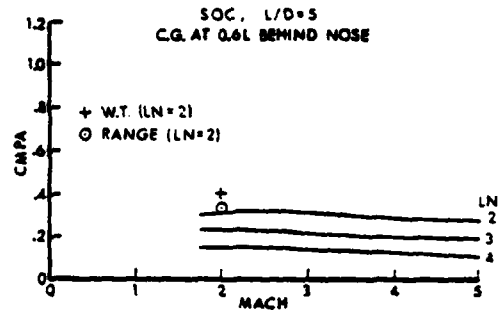


Figure 9. Magnus Moment, Comparison with Experiment

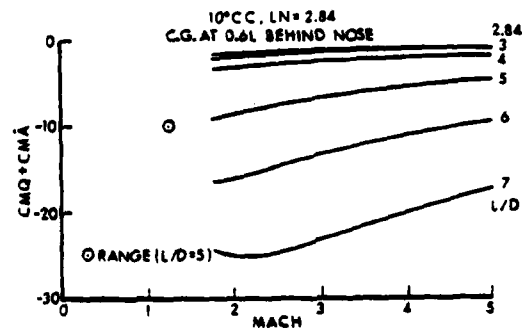


Figure 10. Pitch Damping, Comparison with Experiment

316

Parametric Comparisons

Examples illustrating the parametric results are shown in Figures 11 through 26. The series of comparisons shown in Figures 11 through 20 illustrates an example for each aerodynamic coefficient computed in this study. The case chosen is the SOC model for a total length of six calibers and for ogive lengths of two, three, and four calibers. The aerodynamic coefficients are plotted versus Mach number for atmospheric free stream launch conditions assuming an adiabatic wall temperature boundary condition. These comparisons show, for a fixed body length, that configurations with long slender ogives have reduced pitch damping, less drag, and a reduced Magnus moment compared to bodies with shorter ogive lengths.

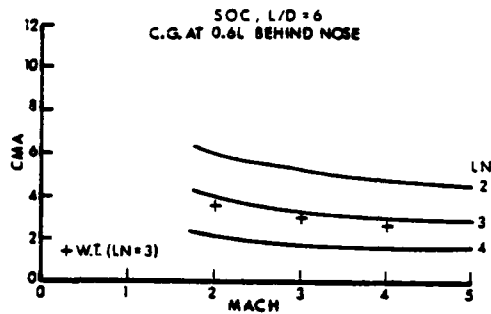


Figure 11. Pitching Moment, Parametric Comparison, SOC, L/D = 6

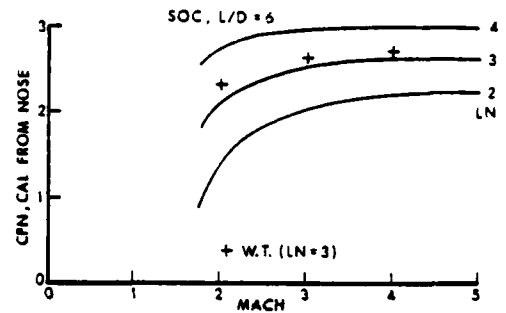


Figure 12. Center of Pressure, Parametric Comparison, SOC, L/D = 6

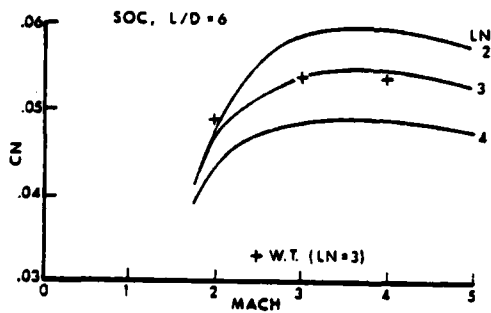


Figure 13. Normal Force, Parametric Comparison, SOC, L/D = 6

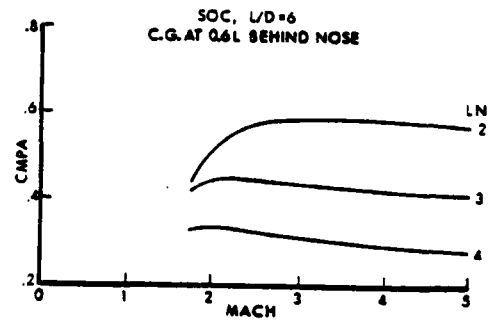


Figure 14. Magnus Moment, Parametric Comparison, SOC, L/D = 6

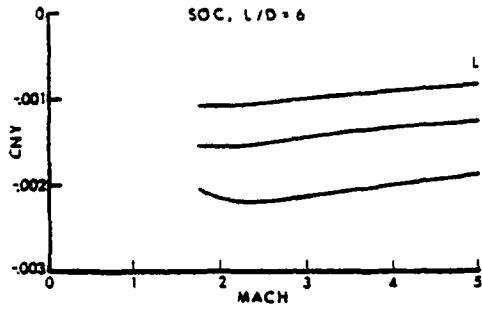


Figure 15. Magnus Force, Parametric Comparison, SOC, L/D = 6

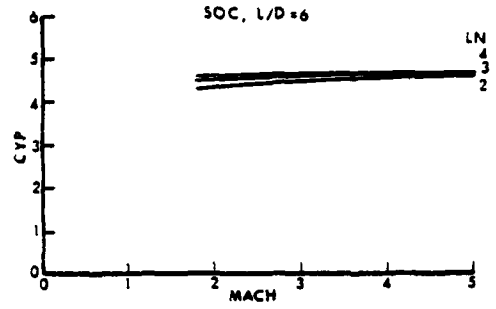


Figure 16. Magnus Center of Pressure, Parametric Comparison, SOC, L/D = 6

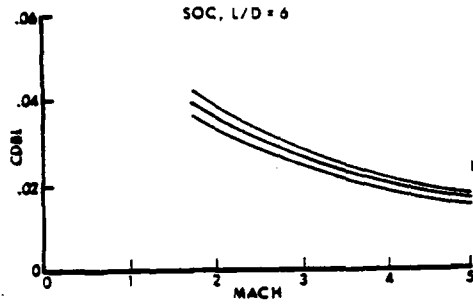


Figure 17. Viscous Drag, Parametric Comparison, SOC, L/D = 6

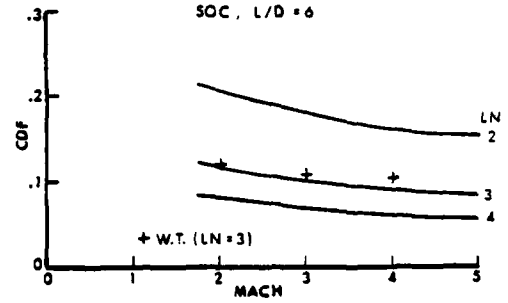


Figure 18. Form Drag Plus Viscous Drag, Parametric Comparison, SOC, L/D = 6

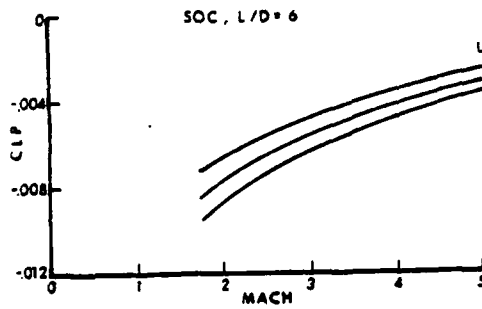


Figure 19. Roll Damping, Parametric Comparison, SOC, L/D = 6

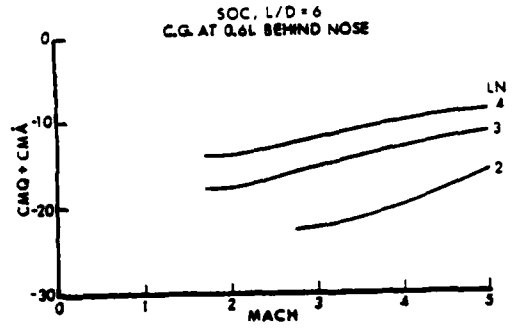


Figure 20. Pitch Damping, Parametric Comparison, SOC, L/D = 6

318

Examples are shown in Figures 21 through 23 illustrating the effects of variations in ogive shape for fixed forebody and total projectile lengths. These comparisons show that pitching moment, Magnus moment, and pitch damping are increased as ogive bluntness is increased.

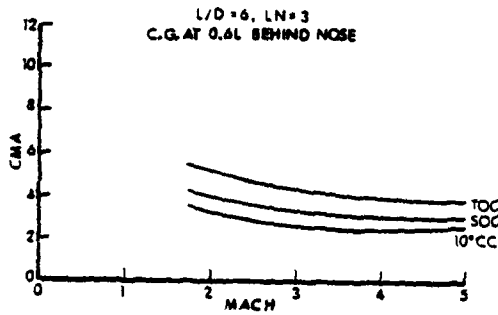


Figure 21. Pitching Moment, Parametric Comparison, $L/D = 6$, $L_N = 3$

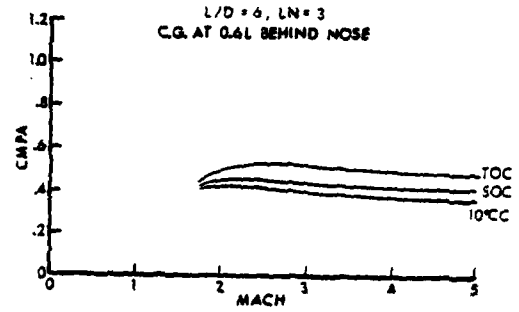


Figure 22. Magnus Moment, Parametric Comparison, $L/D = 6$, $L_N = 3$

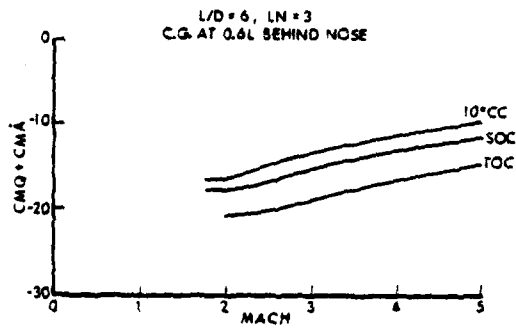


Figure 23. Pitch Damping, Parametric Comparison, $L/D = 6$, $L_N = 3$

The final sequence of parametric comparisons is shown in Figures 24 through 26 where the effect of varying the body length is shown for a fixed ogive shape. These figures show that pitching moment, Magnus moment, and pitch damping are all increased as the body length is increased.

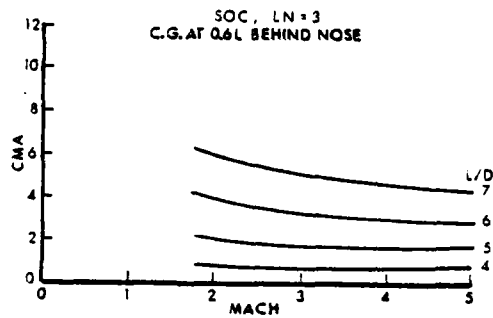


Figure 24. Pitching Moment, Parametric Comparison, SOC, $L_N = 3$

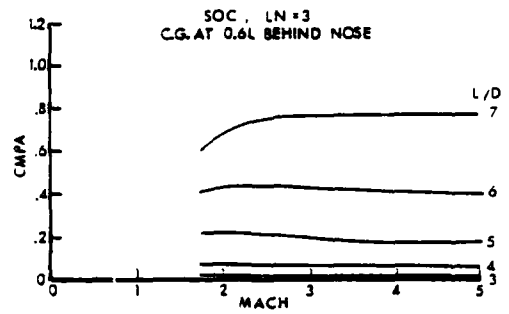


Figure 25. Magnus Moment, Parametric Comparison, SOC, $L_N = 3$

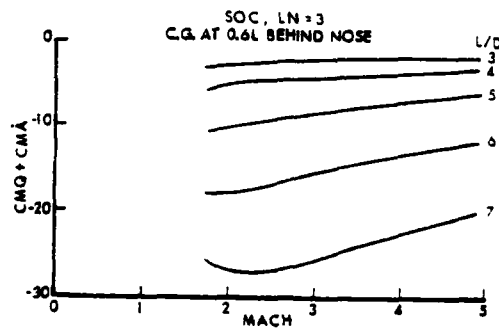


Figure 26. Pitch Damping, Parametric Comparison, SOC, $L_N = 3$

320

The comparisons shown represent a small fraction of the potential comparisons possible from the total data base generated. The intent here has been to illustrate the capability of the computation techniques rather than develop any conclusion as to the relative superiority of any particular configuration. This study is part of a continuing effort that is being expanded to include boattail configurations and a wider Mach number range--transonic velocities are of particular interest.

IV. SUMMARY

A computational aerodynamics parametric study has been described in which advanced numerical techniques for computing three-dimensional inviscid and turbulent viscous supersonic flow fields have been used. A comprehensive data base has been generated for cone-cylinder, tangent-ogive-cylinder, and secant-ogive-cylinder configurations. Comparisons between the computed results and experiment have provided verification of the computational techniques. Comparisons of the computed results for differing body configurations have established the ability of the computation techniques to distinguish the effects of body configuration on the aerodynamic coefficients.

The comparisons for this study represent the first comprehensive use of advanced flow field computation techniques to develop a parametric aerodynamic analysis which includes turbulent viscous effects. Of particular interest are the computations of Magnus effects, which are accomplished in a conceptually exact manner, and the computations of pitch damping. Although the technique of computing pitch damping from a steady coning motion has been available for several years, this study is the first known comprehensive application of this technique to ogive-cylinder bodies.

REFERENCES

1. R. H. Whyte, "Spinner- A Computer Program for Predicting the Aerodynamic Coefficients of Spin Stabilized Projectiles", General Electric Class 2 Reports, 1969.
2. F. G. Moore and C. W. McKerley, "Aerodynamics of Guided and Unguided Weapons; Part II-Computer Program and Usage", NWL TR-3036, 1974.
3. F. G. Moore and Roy C. Swanson, "Aerodynamics of Tactical Weapons to Mach Number 3 and Angle of Attack 15°, Part I- Theory and Application", NSWC/DL TR-3584, February 1977.

STUREK, MYLIN & BUSH

4. H. A. Dwyer and B. R. Sanders, "Magnus Forces on Spinning Supersonic Cones. Part I: The Boundary Layer", AIAA Journal, Vol. 14, April 1976, pp. 498-504.
5. F. N. Moore, "Displacement Effect of a Three-Dimensional Boundary Layer", NACA TN 2722. June 1952.
6. R. W. MacCormack, "The Effect of Viscosity in Hypervelocity Impact Cratering", AIAA Paper 69-364, 1969.
7. B. R. Sanders and H. A. Dwyer, "Magnus Forces on Spinning Supersonic Cones. Part II: The Inviscid Flow", AIAA Journal, Vol. 14, May 1976, pp. 576-582.
8. L. B. Schiff, "Nonlinear Aerodynamics of Bodies in Coning Motion", AIAA Journal, Vol. 10, No. 11, November 1972, pp. 1517-1522.
9. W. B. Sturek, et al, "Computations of Magnus Effects for a Yawed", Spinning Body of Revolution", AIAA Journal, Vol. 16, No. 7, July 1978, pp. 687-692.

NOMENCLATURE

- A = reference area = $\pi D^2/4$
- CDBL = viscous drag = $(\iint \tau_x \cos \theta_B dS)/qA$
- CDF = total drag = $(\iint p_w \sin \theta_B dS)/qA + CDBL$
- CLP = roll damping = $(\iint r \tau_\phi dS)/(qAD PD/V)$
- CM = pitching moment = $(\iint z p_w \cos \phi \cos \theta_B dS)/qAD$
- CMA = pitching moment coefficient = CM/α
- CMPA = Magnus moment coefficient = $CMY/(PD/V/\alpha)$
- CMY = Magnus moment = $[\iint (z p_w \sin \phi \cos \theta_B + z \tau_\phi \cos \phi \cos \theta_B + z \Delta p \sin \phi \cos \theta_B + z \tau_x \sin \phi \sin \theta_B) dS]/(qAD)$
- CN, C_N = normal force = $(\iint p_w \cos \phi \cos \theta_B dS)/qA$
- CMQ + CMA = pitch damping = $C_{n\dot{\theta}}/\sin \alpha$
- CNY, C_Y = Magnus force = $[\iint (p_w \sin \phi \cos \theta_B + \tau_\phi \cos \phi \cos \theta_B + \Delta p \sin \phi \cos \theta_B + \tau_x \sin \phi \sin \theta_B) dS]/qA$

322

STUREK, MYLIN & BUSH

$C_{Y\dot{\theta}}$	= side force in coning motion = $(\int p_w \sin\phi \cos\theta_B dS) / (qA\dot{\theta})$
CPN	= center of pressure = CM/CN
CPY	= Magnus center of pressure = CMY/CNY
D	= diameter of model
P	= spin rate, rad/s
q	= free stream dynamic pressure = $(\rho_\infty V_\infty^2) / 2$
r	= local radius of model
Re_ℓ	= Reynolds number based on model length
S	= surface area
u, v, w	= velocities in boundary-layer coordinates
V	= velocity along model trajectory
x	= surface coordinate in longitudinal direction
y, Y	= coordinate perpendicular to local surface
z	= cylindrical coordinate along model axis
Δp	= centrifugal pressure gradient contribution to side force
σ	= effective angle of attack for coning motion
τ_x	= longitudinal velocity wall shear
τ_ϕ	= circumferential velocity wall shear
θ_B	= local slope of body surface
$\dot{\theta}$	= coning rate

323 - 324x